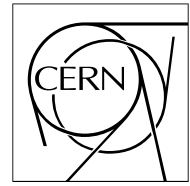


The Compact Muon Solenoid Experiment

# CMS Note

Mailing address: CMS CERN, CH-1211 GENEVA 23, Switzerland



30 May 2006

## Search for a neutral Higgs boson with WH / ZH, $H \rightarrow \gamma\gamma$ channel

M. Lethuillier, O. Ravat, J.-L. Agram, C. Baty, S. Gascon-Shotkin, S. Perriès

*Institut de Physique Nucléaire de Lyon, CNRS-IN2P3, Université Lyon 1, F69622 Villeurbanne*

### Abstract

The associated productions WH and ZH of a Higgs boson decaying into a photon pair are studied using a full detector simulation, with systematic uncertainties taken into account. One year of LHC running at high luminosity (integrated luminosity of  $100 \text{ fb}^{-1}$ ) allows an observation at  $3\sigma$  of the SM Higgs boson from the LEP lower limit up to  $146 \text{ GeV}/c^2$ . Three years of running at high luminosity allows a  $5\sigma$  discovery from the LEP lower limit up to  $148 \text{ GeV}/c^2$ . In addition, this channel may be one of the recovery channels in case of a light higgs gluophobic scenario.

# 1 Introduction

Compared to the gluon-gluon fusion channel  $gg \rightarrow H \rightarrow \gamma\gamma$  [1], the associated production channels WH/ZH suffer from a much lower production cross section. Several advantages, however, make these channels attractive when the decay of the gauge boson results in a charged lepton: requiring an additional relatively high transverse-momentum lepton greatly reduces the significant QCD background in the  $\gamma\gamma$  topology and improves the primary vertex reconstruction [2]. In the context of supersymmetric models, maximal mixing in the stop sector could result in a strong suppression of the  $gg \rightarrow h$  signal, which the associated production channels would not be subject to [3]. The searched-for final state comprised of 2 isolated photons and at least one isolated electron or muon is close to that of the other associated production channel  $t\bar{t}H$  [4]. The 2-photon signature of a Higgs boson decay has also been studied in association with two forward jets [5]. After one year of high luminosity running, from 88 to 25 events  $WH \rightarrow l\nu\gamma\gamma$  (with  $l = e$  or  $\mu$ ) and from 15 to 4 events  $ZH \rightarrow ll\gamma\gamma$  (with  $l = e$  or  $\mu$ ) are expected for Higgs boson masses in the range  $115 - 150 \text{ GeV}/c^2$ . Prior generator-level studies in the context of the Standard Model [6] and of the MSSM [7] show the possibility of a discovery in this channel. This was confirmed by two ATLAS studies, using a fast simulation, published in [8, 9]. The results presented in this note are the continuation of the work documented in [10].

## 2 Event generation and preselection

All the processes considered in this study have been simulated at the leading order. Signal events were generated by the matrix element generator COMPHEP [11] for Higgs boson masses ranging from 90 to  $150 \text{ GeV}/c^2$ , in steps of  $5 \text{ GeV}/c^2$ . At each mass value, 10000 events were generated. Total cross-sections have been rescaled accordingly to the NLO calculation [12]. K-factors from 1.15 to 1.16 are obtained on the whole mass range. Branching ratios for  $H \rightarrow \gamma\gamma$  were taken from HDECAY program [13]. The irreducible backgrounds from the processes  $W\gamma\gamma$  et  $Z\gamma\gamma$  were also generated with COMPHEP, with the same K-factors applied as those pertinent to the signal. Fragmentation and hadronization was performed by PYTHIA [14].

The following five most significant reducible backgrounds were retained due to their capacity to mimic the  $l\gamma\gamma$  signal:

- $\gamma$ -jet production: one prompt photon, one lepton faked within a jet or from a semi-leptonic decay of B meson, and the other photon either radiated by the outgoing quark, or faked by a  $\pi^0$  (or  $\eta, \omega$ ) within a jet;
- $\gamma\gamma$  prompt diphoton production from gluon fusion or quark annihilation: the lepton is either a fake or a B semi-leptonic decay from a jet radiated in the initial state;
- $W\gamma$  production: one prompt photon, one lepton coming from the W decay, and the other photon either radiated by the lepton or faked in a jet radiated by one of the initial quarks;
- $t\bar{t}$  pair production: one lepton from a leptonic decay of a W, and the two photons are either a bremsstrahlung of a top, or radiated by the lepton, or a fake within a jet, or an electron coming from the other W or from a semileptonic decay of B meson and of which track was not assigned to the calorimeter cluster;
- $b\bar{b}$  pair production: the lepton is coming from one semileptonic decay, one photon may be radiated by this lepton, and most probably the two photons are mimicked by neutral hadrons within jets. The probability to get two isolated photons is much smaller compared to other backgrounds, but is largely compensated by the very high cross-section.

All these backgrounds have been generated with PYTHIA and leading order cross-sections are considered, except for the  $t\bar{t}$  production where a NLO cross section of 840 pb is used [15].

To ensure an efficient generation and preserve sufficient statistics of the most signal like events, a preselection is applied at generator level. Three electromagnetic candidates or two electromagnetic candidates and one muon candidate with  $E_T > 20 \text{ GeV}$  and  $|\eta| < 2.7$  are required. For backgrounds generated with PYTHIA, an electromagnetic candidate is obtained by clustering electrons and photons in a  $\Delta\eta = 0.09, \Delta\phi = 0.09$  window. Muon candidates are either  $\mu, \tau, \pi, \text{ or } K$  particles. The cross-sections, the number of generated and preselected events and the statistical weight for each reducible background are given in Table 1. For backgrounds generated with COMPHEP, the electromagnetic and muon candidates are simply the photons and the electron or muon from the hard process. The selection at this level is necessary to avoid divergence problems in COMPHEP.

Table 1: Preselection at generator level for reducible backgrounds.

	$\hat{p}_T$ bin (GeV/c)	Cross-section (pb)	Number of generated events	Number of preselected events	Equivalent luminosity (fb <sup>-1</sup> )
$\gamma\gamma$	30-100	107.8	$6.4 \cdot 10^7$	139 500	597
$\gamma\gamma$	> 100	1.95	$5.9 \cdot 10^6$	109 500	3 008
W $\gamma$	30-100	5.54	$2.0 \cdot 10^7$	80 000	3 683
W $\gamma$	> 100	0.25	$1.1 \cdot 10^6$	20 000	4 181
$b\bar{b}$	30-100	$1.8 \cdot 10^6$	$4.6 \cdot 10^8$	25 323	0.26
$b\bar{b}$	> 100	$1.3 \cdot 10^4$	$5.2 \cdot 10^6$	80 000	0.40
$t\bar{t}$	–	86.2	$1.2 \cdot 10^6$	80 000	13.3
$\gamma$ -jet	30-100	$1.2 \cdot 10^5$	$1.7 \cdot 10^7$	5 726	0.14
$\gamma$ -jet	> 100	$1.8 \cdot 10^3$	$4.4 \cdot 10^6$	79 873	2.52

### 3 Event reconstruction

The events were generated assuming a pile-up rate corresponding to high luminosity phase ( $\mathcal{L} = 10^{34} \text{ cm}^{-2}\text{s}^{-1}$ ). Full detector simulation and reconstruction has been used, based on GEANT 3 [17].

### 4 Trigger selection

The default trigger tables at high luminosity are used. Events are required to pass the global Level 1 trigger [19]. Only the double photon stream of the High Level Trigger (HLT) is selected [20]. The transverse energy thresholds are asymmetric and set to 35 and 20 GeV/c. The trigger efficiencies for the preselected signal events are higher than 95% on the whole Higgs boson mass range (90 to 150 GeV/c<sup>2</sup>). The efficiencies reach 98% for signal events preselected with three electromagnetic candidates and 92% for those preselected with two electromagnetic candidates and one muon candidate. The number of events passing the trigger selection is given in Table 3 for signal and irreducible backgrounds and in Table 4 for reducible backgrounds.

## 5 Offline event selection

### 5.1 Analysis method

The goal of the first part of the analysis is to eliminate the maximum possible number of reducible background events with large statistical weight (especially  $b\bar{b}$  and  $\gamma$ -jet backgrounds).

A very loose preselection is applied: at least two offline photons and one electron or muon has to be reconstructed by the standard algorithms. Four discriminant combined variables are then constructed using a likelihood ratio method to estimate:

- the isolation of the photons
- the quality of the lepton reconstruction
- the isolation of the lepton
- the QCD / multi-jets nature of the event

The reference histograms for the four likelihoods are all produced on independent simulated event samples at this same level of preselection. The input reference histograms used in the likelihood are not produced consecutively (*i.e.* not produced with the subset of events selected by the cut on the previous likelihood) in order to limit the integrated luminosity necessary for an optimization of the likelihood based on real data taken from the  $m_{\gamma\gamma}$  sidebands as it will be shown in section 6.1. The expected rates of signal and background events at this level are given in Table 2.

Table 2: Cross-section times branching ratio times selection efficiency after the loose preselection applied before the four likelihood calculations. The preselection requires two offline photons and one offline electron or muon.

	WH	ZH	W $\gamma\gamma$	Z $\gamma\gamma$	$\gamma\gamma$	W $\gamma$	$b\bar{b}$	$t\bar{t}$	$\gamma$ -jet
$\sigma \times \text{BR} \times \epsilon$ (fb)	0.373	0.040	7.038	7.681	56.9	13.6	63524	1714	21495

Sequential cuts are then applied on these 4 discriminant variables. After the strong suppression of multi-jets backgrounds ( $b\bar{b}$ ,  $t\bar{t}$  and  $\gamma$ -jet), some kinematical variables (lepton/photon angles and momentum, magnitude and direction of the missing transverse energy) can be used and combined into a final likelihood to discriminate more signal-like backgrounds ( $W\gamma\gamma$ ,  $Z\gamma\gamma$ ,  $\gamma\gamma$ ,  $W\gamma$ ). No kinematical variable is used in the 4 first likelihoods to avoid correlations between these variables and the di-photon mass since it would degrade the performance of the likelihood optimization in the  $m_{\gamma\gamma}$  sidebands.

## 5.2 Photon reconstruction and isolation

Photons are reconstructed with the standard CMS offline algorithms. Photon candidates with a matching seed in the pixel detector are rejected. The two photons with the highest transverse energy are selected. The photon candidates identified in multijet background events come largely from neutral hadrons ( $\pi^0$ ,  $\eta$ ,  $\omega$ ) within the jets. Photons produced in the decays of these hadrons are strongly collinear with the jet direction. Therefore electromagnetic and hadron calorimeter isolation should permit strong discrimination between these hadron-decay photons and prompt isolated signal photons. Detailed studies of the photon isolation criteria have been previously carried out for the  $H \rightarrow \gamma\gamma$  inclusive analysis [22, 23]. Several variables which estimate the calorimetric energy in the neighbourhood of a photon were tested:

- ECAL SimpleCone: Sum the transverse energy of the basic clusters (reconstructed with the ‘‘island’’ algorithm [21]) within a cone  $\Delta R < 0.3$  around the photon, excluding the basic clusters belonging to the photon supercluster (see Figure 1);
- ECAL BiCone: Sum the transverse energy of the island basic clusters within a double cone  $0.08 < \Delta R < 0.3$  centred on the photon (see Figure 2);
- SCISO: Sum the transverse energy of the island basic clusters within a double cone  $0.08 < \Delta R < 0.35$  centred on the photon, excluding the basic clusters in a  $|\Delta\eta| < 0.03$  band (see Figure 3). This isolation variable is similar to the one used by default for electromagnetic objects in ORCA The Phi ring is used to exclude from the isolation method the clusters due to the bremsstrahlung;
- HCAL Iso: Sum of the transverse energy of the HCAL towers within a cone  $\Delta R < 0.3$  around the photon (see Figure 4);
- HCAL nTowers: Number of HCAL towers hit within a cone  $\Delta R < 0.3$  around the photon (see Figure 5).

The use of isolation criteria involving the pixel detector was also considered. This enables slightly increased discrimination power but at the price of a non-negligible loss in signal efficiency. Since the goal is to preserve the highest efficiency possible before entering the second part of the analysis (use of kinematical variables), the criteria were not adopted.

To combine the isolation variables, a likelihood ratio method is used. For each observable  $x_i$ , the likelihood ratio  $\mathcal{L}_i(x_i)$  is defined as:

$$\mathcal{L}_i(x_i) = \frac{f^S(x_i)}{f^B(x_i)}$$

where  $f^S$  and  $f^B$  are the probability density functions for the signal and the background. A global discriminant variable  $y$  is then constructed as the product of the individual likelihood ratios  $\mathcal{L}_i(x_i)$ . Theoretically, the combination of several discriminant variables is optimal only if multidimensional functions are used in the likelihood ratio. Nevertheless, with weakly correlated variables, we will do the following approximation:

$$y = \frac{f^B(x_1, \dots, x_n)}{f^S(x_1, \dots, x_n)} \simeq \frac{f^B(x_1) \times \dots \times f^B(x_n)}{f^S(x_1) \times \dots \times f^S(x_n)} = \prod_{i=1}^n \mathcal{L}_i(x_i)$$

Another approach is to apply weights to the individual likelihood ratio to take into account the correlations [24]. To search for the best performance, the curves giving the signal efficiency versus the expected background (obtained by varying the cut on  $y$ ) are compared for different combinations of variables, retaining those which yield the best rejection accompanied by high signal efficiency (90 – 95%). The best performance is obtained with a combination of the ECAL SimpleCone and the HCAL Iso variables for both photons. The distribution of the resulting discriminant variable  $y_1$  is shown in Figure 6. We apply the criterion  $\log(y_1) > -0.4$  which is particularly effective against  $b\bar{b}$  pair production (rejection factor of 76) as well as against top quark pair production (rejection factor of 30). On the other hand the background  $\gamma$ -jet is only reduced by a factor of 4 due to the presence of genuine isolated photon.

### 5.3 Quality of the lepton reconstruction

The standard offline algorithms are used to reconstruct the electrons and the muons. Sometimes several tracks are matching the same electron supercluster. The track with the momentum closest to the supercluster energy is chosen. The lepton candidate is then defined as the electron or muon with respectively the highest  $E_T$  measured by the electromagnetic calorimeter or  $p_T$ . We then seek to verify good reconstruction quality for the lepton candidate and to reject fake leptons produced within jets. In the case of multijet events, the density of particles within a jet is such that the calorimetric deposits from photons or neutral hadrons are frequently erroneously associated with a track and are wrongly identified as electrons.

Numerous variables involving the calorimetry and the tracker system were tested. The four variables yielding the most significant discriminating power are:

- $E_{em}/p$ : the ratio between the electron energy as measured in the electromagnetic calorimeter and its momentum measured by the tracker. This ratio should tend towards 1 when the calorimetric deposit has been correctly associated to a track. The distribution of this variable is shown in Figure 7;
- $E_{had}/E$ : the hadronic energy fraction;
- $\Delta\eta$  trk-clus: The distance in  $\eta$  between the track and the associated supercluster. This value should tend towards 0 in the case of a correct association. The angle in phi is not considered due to bremsstrahlung. Under the influence of the magnetic field, the electron tends to distance itself in phi from the radiated photons. The distribution of this variable is shown in Figure 8;
- r9: The ratio between the sum of the energies of 9 crystals (3x3 matrix centred on the maximum-energy crystal) and the energy of the corresponding supercluster. This ratio is related to the shower shape. Electrons having experienced little bremsstrahlung have their energy concentrated in the shower center (see Figure 9).

The four variables are combined in a likelihood. The distribution of the output variable  $y_2$  is shown in Figure 10. A cut  $\log(y_2) > -0.6$  is applied.

In the case of muons the purity obtained by the standard CMS reconstruction algorithms has already proven sufficient; therefore, no additional criteria are applied.

### 5.4 Lepton isolation

In most of the reducible backgrounds, the identified lepton is a fake lepton or a lepton from a B semi-leptonic decay within a jet, far less isolated than a lepton coming from a W or Z decay. The same variables as those studied for photons are tested. For the electron, the method is quite similar to the photon case. For muons, the muon track is extrapolated through the magnetic field to the calorimeter. The only difference is that no cluster is associated to the muon, so no basic clusters are removed during the calculation of the ECAL SimpleCone variable and the energy deposited by the muon in the calorimeter is not subtracted. That is why the ECAL BiCone variable offers better performance than the SimpleCone one. The best combination is obtained with (ECAL BiCone + HCAL Iso). The distributions are presented in Figures 11 and 12. In addition, the number of pixel lines within a cone  $\Delta R < 0.3$ , presented in Figure 13 improves the discriminative power of the likelihood. In the future, some performance improvement of the lepton isolation is expected by using the full tracker information as it was done in [24]. The distribution of the output variable  $y_3$  of the likelihood is shown in Figure 14. A cut  $\log(y_3) > -0.3$  is applied.

### 5.5 Multi-jet events rejection

The rejection of  $\pi^0$  faking signal photons, effective against QCD backgrounds, has been accomplished by a neural net procedure exploiting the information on the lateral profile of the electromagnetic shower. The distributions of the discriminant variable for the two photon candidates are shown in Figures 15 and 16.

Variables involving the multiplicity of reconstructed objects in the electromagnetic calorimeter reinforce the discriminating power. In particular, the number of seed clusters reconstructed by the island algorithm, as shown in Figure 17. The distribution of the combined variable  $y_4$  obtained by a likelihood ratio method is given in Figure 18. A cut  $\log(y_4) > -0.8$  is applied on this variable.

Table 3: Production cross-section times branching ratio, and cross-section times branching ratio times preselection efficiency after each stage of the event selection for signals ( $m_H = 120 \text{ GeV}/c^2$ ) and irreducible backgrounds. All values are shown in fb. Errors are statistical only.

	WH	ZH	W $\gamma\gamma$	Z $\gamma\gamma$
$\sigma \times \text{BR}$	0.810	0.137	-	-
Preselection: $\sigma \times \text{BR} \times \epsilon$	0.460	0.0440	13.58	18.92
Double photons HLT	$0.439 \pm 0.005$	$0.0423 \pm 0.0004$	$8.80 \pm 0.04$	$12.13 \pm 0.07$
At least 2 offline photons	$0.415 \pm 0.005$	$0.0400 \pm 0.0004$	$8.23 \pm 0.04$	$10.01 \pm 0.06$
$E_T(\gamma_1) > 35 \text{ GeV}$	$0.411 \pm 0.005$	$0.0394 \pm 0.0004$	$7.47 \pm 0.04$	$7.30 \pm 0.05$
Photons isolation	$0.387 \pm 0.005$	$0.0370 \pm 0.0004$	$7.14 \pm 0.04$	$6.51 \pm 0.04$
At least 1 offline lepton	$0.348 \pm 0.004$	$0.0362 \pm 0.0003$	$5.94 \pm 0.04$	$4.80 \pm 0.03$
Lepton quality	$0.331 \pm 0.004$	$0.0350 \pm 0.0003$	$5.56 \pm 0.04$	$4.58 \pm 0.03$
Lepton isolation	$0.299 \pm 0.004$	$0.0318 \pm 0.0003$	$4.83 \pm 0.04$	$4.11 \pm 0.03$
QCD rejection	$0.281 \pm 0.004$	$0.0273 \pm 0.0003$	$4.50 \pm 0.04$	$3.53 \pm 0.03$
$\Delta R(\gamma\gamma l) > 0.3$	$0.281 \pm 0.004$	$0.0272 \pm 0.0003$	$4.49 \pm 0.04$	$3.52 \pm 0.03$
$80 < m_{\gamma\gamma} < 160$	$0.271 \pm 0.004$	$0.0259 \pm 0.0003$	$2.04 \pm 0.02$	$1.42 \pm 0.02$

Table 4: Production cross-section times branching ratio, and cross-section times branching ratio times preselection efficiency after each stage of the event selection for reducible backgrounds. Contributions of the different  $p_T$  bins are summed. All values are shown in fb. Errors are statistical only.

	$\gamma\gamma$	W $\gamma$	b $\bar{b}$	t $\bar{t}$	$\gamma$ -jet (jet)
$\sigma \times \text{BR}$	$1.1 \times 10^5$	$5.79 \times 10^3$	$1.78 \times 10^9$	$86.2 \times 10^3$	$1.21 \times 10^8$
Preselection: $\sigma \times \text{BR} \times \epsilon$	270.1	26.5	$2.96 \times 10^5$	$6.00 \times 10^3$	$7.16 \times 10^4$
Double photons HLT	$197.7 \pm 1.0$	$16.8 \pm 0.1$	$77120 \pm 764$	$1948 \pm 17$	$35045 \pm 256$
At least 2 offline photons	$194.4 \pm 1.0$	$15.2 \pm 0.1$	$71935 \pm 738$	$1872 \pm 17$	$32038 \pm 244$
$E_T(\gamma_1) > 35 \text{ GeV}$	$187.0 \pm 0.9$	$13.6 \pm 0.09$	$51991 \pm 627$	$1069 \pm 13$	$31098 \pm 241$
Photons isolation	$161.6 \pm 0.8$	$9.97 \pm 0.07$	$682 \pm 72$	$31.2 \pm 2.2$	$7235 \pm 115$
At least 1 offline lepton	$39.1 \pm 0.4$	$8.52 \pm 0.07$	$523 \pm 63$	$27.0 \pm 2.0$	$4751 \pm 93$
Lepton quality	$27.3 \pm 0.3$	$7.98 \pm 0.07$	$311 \pm 49$	$23.5 \pm 1.9$	$2552 \pm 68$
Lepton isolation	$9.8 \pm 0.2$	$6.59 \pm 0.06$	(0.87)	$14.2 \pm 1.5$	$209 \pm 20$
QCD rejection	$7.6 \pm 0.2$	$5.74 \pm 0.06$	(0.003)	(0.35)	(6.6)
$\Delta R(\gamma\gamma l) > 0.3$	$7.6 \pm 0.2$	$5.70 \pm 0.06$	(0.002)	(0.31)	(5.3)
$80 < m_{\gamma\gamma} < 160$	$3.2 \pm 0.1$	$2.40 \pm 0.04$	(0.001)	(0.26)	(3.7)

## 5.6 Kinematical selection - Final likelihood

The results of the sequential cuts applied on the 4 combined variables are presented in Tables 3 and 4. The multijet backgrounds are entirely suppressed. The cut factorisation method is applied in order to estimate the contribution of these backgrounds which are reduced to zero due to finite statistics. The photon isolation criteria is temporarily removed in order to estimate the efficiencies of the last cuts (lepton isolation and beyond). These efficiencies are then applied to the number of events remaining before the cuts which have removed all of them. The estimations obtained by this method are indicated between parentheses in Tables 3 and 4. After rejecting events outside the 80-160  $\text{GeV}/c^2$  di-photon mass window, the expected rate of events is:

$$\sigma \times \text{BR} \times \epsilon (\text{Signal}) = 0.297 \pm 0.003 \text{ fb}$$

$$\sigma \times \text{BR} \times \epsilon (\text{Background}) = 13.1 \pm 2.6 \text{ fb}$$

Some simple kinematical variables are used to form a final likelihood. The reference S/B histograms are produced using half of the statistics available after the sequential selection (35990 MC events for signals and 10630 MC events for background). The more discriminant variables have been identified such as the transverse energy of the photons (see Figures 19 and 20), the transverse calorimeter energy of the electron or the transverse momentum of the muon (see Figure 21), the  $\Delta R$  distances between lepton and each photon (see Figures 22 and 23). The  $\Delta R$  distances between the two photons (see Figure 24) is strongly correlated with the di-photon reconstructed mass used to derive the statistical significances, so it is not kept in the final likelihood. The missing transverse energy <sup>1)</sup> also improves the discrimination, in particular its magnitude (see Figure 25) and its phi angle (see Figure 26) with the direction of the first photon. The distribution of the resulting combined variable  $y_5$  is shown in Figure 27 for a Higgs boson mass of 120  $\text{GeV}/c^2$ .

<sup>1)</sup> The missing transverse energy was calculated using the Iterative Cone Algorithm for jet clustering with a cone size of 0.6 and a  $p_T > 15 \text{ GeV}/c$  threshold for the jets.

## 5.7 Statistical method and optimization

The statistical methods developed by the LEP Higgs working group [25] are used in this analysis to optimize the selection criteria and determine the statistical significance of the final results. It will never be possible to exclude with an absolute certainty the presence or absence of a signal (In the following, the background-only hypothesis (the null hypothesis) will be noted  $b$  and  $s + b$  will be used for the signal+background hypothesis). Therefore a Confidence Level (CL) is introduced to characterize the statistical significance of the exclusion or discovery. The first step to obtain this CL is to select the most discriminating observables. These variables are then used to construct the test-statistic  $X$  which classifies the experiments according to their more or less background like or signal+background like nature. The test-statistic will also be used to determine the confidence level to exclude the  $b$  or  $s + b$  hypothesis.

**Test-statistic** - the test-statistic is chosen to increase monotonically for more signal like experiments. The probability of rejecting a false hypothesis at a given confidence level is maximized by using a likelihood ratio as test-statistic:

$$X = \frac{\mathcal{L}_{s+b}}{\mathcal{L}_b}$$

The most obvious information which has to be introduced into the likelihood function is the counting rates of the expected signal  $s$  and background  $b$  events. The  $s$  and  $b$  rates follow a Poisson probability:

$$X = \frac{e^{-(s+b)} (s + b)^n / n!}{e^{-b} b^n / n!}$$

where  $n$  is the number of observed events. The separative power of the likelihood function can be improved by the addition of other discriminating variables such as the reconstructed di-photon mass. If this additional variable  $x$  is distributed like  $S(x)$  and  $B(x)$  for respectively the signal and background events then the test-statistic is defined by :

$$\begin{aligned} X &= \frac{e^{-(s+b)} (s + b)^n / n!}{e^{-b} b^n / n!} \frac{\prod_{j=1}^n \frac{sS(x_j) + bB(x_j)}{s+b}}{\prod_{j=1}^n B(x_j)} \\ &= e^{-s} \prod_{j=1}^n \left( 1 + \frac{sS(x_j)}{bB(x_j)} \right) \end{aligned}$$

This result is easily extended to the case of a multi-channel search:

$$X = e^{-s_{tot}} \prod_{i=1}^N \prod_{j=1}^{n_i} \left( 1 + \frac{s_i S_i(x_{ij})}{b_i B_i(x_{ij})} \right)$$

where  $N$  is the number of channels to be considered,  $n_i$  the number of observed candidates in the channel  $i$ ,  $s_i$  and  $b_i$  the expected signal and background rates for the channel  $i$ ,  $s_{tot}$  the total expected number of signal events,  $x_{ij}$  the value of the discriminating variable obtained for the candidate  $j$  of channel  $i$ ,  $S_i$  and  $B_i$  the probability density functions of the discriminating variable for the signal and the background of the channel  $i$ .

**Definition of the Confidence Level** - The test-statistic  $X$  increases monotonically for increasingly signal-like experiments. The CL in the  $s + b$  hypothesis can therefore be defined as the probability that a  $s + b$  experiment gives a value  $X$  of the test-statistic lower than the observed  $X_{obs}$  :

$$CL_{s+b} = \mathcal{P}_{s+b}(X \leq X_{obs}) = \int_0^{X_{obs}} \frac{d\mathcal{P}_{s+b}}{dX} dX$$

where  $d\mathcal{P}_{s+b}/dX$  is the probability density function of the test-statistic in the case of signal+background experiments. The confidence level in the null hypothesis is defined by:

$$\text{CL}_b = \mathcal{P}_b(X \leq X_{obs}) = \int_0^{X_{obs}} \frac{d\mathcal{P}_b}{dX} dX$$

A  $5\sigma$  discovery will be established when the probability  $1 - \text{CL}_b$  that a background only experiment gives a more signal like result than the observation is less than  $5.7 \times 10^{-7}$ .

The CL in the signal hypothesis is defined using a modified frequentist renormalization :

$$\text{CL}_s = \text{CL}_{s+b} / \text{CL}_b$$

and the presence of signal will be said to be excluded at a CL equal to  $1 - \text{CL}_s$ .

**Choice of the working point** - To form the test-statistic, the two obvious variables to be used are the reconstructed  $\gamma\gamma$  invariant mass and the kinematical likelihood variable  $y_5$ . The limited statistics of the MC events prohibit however the use of a two-dimensional method for the determination of the Higgs boson discovery potential. So, only the shape of the reconstructed  $\gamma\gamma$  mass distribution will be used along with a cut on the combined likelihood variable  $y_5$ . The choice of the optimal working point (i.e. the  $y_5$  cut value) will be that which maximizes the discovery potential. Figure 28 illustrates the optimization process for  $m_H = 120 \text{ GeV}/c^2$  and an integrated luminosity of  $100 \text{ fb}^{-1}$ . For each tentative cut on the global variable  $y_5$ , the  $m_{\gamma\gamma}$  distribution is drawn for signal and background and is used as input for the confidence level calculation. The statistical significance obtained as a function of the cut on  $y_5$  is shown in Figure 29. The cut on  $y_5$  which maximize the significance is chosen. This optimal working point is a function of the  $m_H$  hypothesis but is independent of the integrated luminosity, as far as systematic uncertainties are not taken into account. So, the statistical significance can be easily traced as a function of the luminosity as shown in Figure 36 for all  $m_H$  hypothesis. The list of the optimal working points obtained for the different Higgs boson mass hypotheses is given in Table 5. The significance and the expected number of signal and background events are given for a luminosity of  $100 \text{ fb}^{-1}$ . For the  $\gamma$ -jet,  $t\bar{t}$  and  $b\bar{b}$  backgrounds, the rate is estimated by the method of cut factorization described in section 5.6.

Table 5: Optimal working points for the different Higgs boson mass hypotheses. The significance and the expected number of signal and background events are given for an integrated luminosity of  $100 \text{ fb}^{-1}$ .

$m_H$ (GeV/ $c^2$ )	working point $\log(y) >$	significance	WH	ZH	W $\gamma\gamma$	Z $\gamma\gamma$	W $\gamma$	$\gamma\gamma$	$\gamma$ -jet	$t\bar{t}$	$b\bar{b}$
90	0.24	$5.66 \sigma$	38.9	3.2	66.2	42.9	51.6	14.7	1.3	0.37	$13 \times 10^{-5}$
95	0.28	$5.18 \sigma$	34.0	2.8	63.8	37.7	48.8	12.3	1.4	0.28	$13 \times 10^{-5}$
100	0.28	$5.27 \sigma$	32.2	2.6	62.6	39.4	48.2	13.4	1.6	0.30	$16 \times 10^{-5}$
105	0.53	$4.92 \sigma$	25.2	2.2	47.2	26.1	32.2	7.4	1.1	0.19	$7 \times 10^{-5}$
110	0.56	$4.73 \sigma$	22.6	2.0	43.0	25.2	28.3	7.6	1.2	0.16	$7 \times 10^{-5}$
115	0.41	$4.30 \sigma$	22.1	1.8	49.3	30.9	33.0	10.2	1.7	0.16	$10 \times 10^{-5}$
120	0.35	$4.09 \sigma$	20.7	1.6	51.2	36.2	34.5	12.4	1.9	0.15	$10 \times 10^{-5}$
125	0.59	$4.01 \sigma$	17.1	1.4	36.3	21.2	23.6	7.0	1.3	0.12	$7 \times 10^{-5}$
130	0.68	$3.64 \sigma$	14.6	1.3	30.7	16.9	18.7	6.0	1.4	0.10	$4 \times 10^{-5}$
135	0.82	$3.47 \sigma$	13.1	1.2	24.9	13.2	15.0	5.0	1.2	0.07	$3 \times 10^{-5}$
140	0.99	$3.35 \sigma$	11.4	1.0	18.9	10.3	10.6	3.7	1.0	0.04	$1 \times 10^{-5}$
145	1.18	$3.13 \sigma$	9.7	0.8	13.8	6.5	7.9	2.9	0.7	0.03	$< 1 \times 10^{-5}$
150	0.83	$2.87 \sigma$	10.4	0.9	20.2	11.7	12.3	5.4	1.1	0.03	$3 \times 10^{-5}$

## 6 Use of real data in sidebands - Systematic uncertainties

The signal searched for is characterized by a strongly peaked di-photon invariant mass. Furthermore, at the optimal working points, the  $m_{\gamma\gamma}$  distribution of the background is smooth and flat. When real data will be there, this will allow us to use the data taken in  $m_{\gamma\gamma}$  sidebands to optimize the likelihood analysis and to estimate the background.

### 6.1 Likelihood optimization with sideband events

No kinematical observables were used to construct the four primary likelihoods aimed at rejecting multijet events. If the shapes of the distributions of the variables used in the likelihoods are sufficiently similar for different di-

photon mass regions, then data taken outside the signal region can be used to optimize the likelihood. Only the signal MC will be used, and the analysis does not rely on the MC background avoiding the possibly large related uncertainties. To test the method, a sample of “fake real data” is used, i.e. the number of MC events for each background is equal to the expected number of events for a given luminosity. The size of the sample is limited by the equivalent luminosity of the MC samples produced. The same preselection as in the standard analysis is used: two offline photons and one electron or muon are required. The reference S/B histograms for the likelihoods are produced with the events taken in the  $20 < m_{\gamma\gamma} < 80 \text{ GeV}/c^2$  band. The total number of MC events available in this band is given in Table 6. This table also shows that the equivalent integrated luminosity corresponding to the fake data sample is limited to  $132 \text{ pb}^{-1}$  by the statistics available for the  $b\bar{b}$  background. The composition of the sample is given in the last column of Table 6. The dominant contribution of  $b\bar{b}$  events amounts to 87%,  $\gamma$ -jet events represent 9%, and  $t\bar{t}$  events 4%. The reference S/B histograms of the likelihood ratio method are produced with these events and the four global variables  $y_1, y_2, y_3, y_4$  are then calculated for the events in the  $80 < m_{\gamma\gamma} < 160 \text{ GeV}/c^2$  band. The performance is compared to the results obtained in the same  $80 - 160 \text{ GeV}/c^2$  band by the standard analysis optimized with the full MC statistics available without any cut on  $m_{\gamma\gamma}$ . The distributions of the photon isolation combined variable  $y_1$  are shown in Figure 30 for these two cases and Figure 31 illustrates the comparison of the performance obtained by the two methods. For the four global discriminant variables, up to 20% loss of efficiency is observed for the same rejection power. The degradation of the performance is mainly due to the insufficient statistics of  $\gamma$ -jet and  $t\bar{t}$  events in  $132 \text{ pb}^{-1}$  of data:  $\sim 200$   $\gamma$ -jet events is clearly insufficient to get the full discrimination power of the combined variables against this background. To increase the size of the “fake data sample”, gedanken experiments were generated. The absence of correlations between the variables used in the likelihood is assumed. The distributions of these variables in the  $20 < m_{\gamma\gamma} < 80 \text{ GeV}/c^2$  sideband are fitted and used to generate pseudo-experiments. The performance obtained is represented in Figure 31. An integrated luminosity of  $5 \text{ fb}^{-1}$  will be sufficient to optimize the four primary likelihoods with the real data taken in the  $m_{\gamma\gamma}$  sideband and to reproduce the results obtained when using the full MC statistics.

Table 6: Results of the preselection in the  $20 < m_{\gamma\gamma} < 80 \text{ GeV}/c^2$  sideband.

	Nb of selected MC events	$\sigma \times \text{BR} \times \epsilon$ (fb)	Equivalent luminosity ( $\text{fb}^{-1}$ )	Number of events for $132 \text{ pb}^{-1}$
$W\gamma\gamma$	11772	3.393	3469	0
$Z\gamma\gamma$	21805	4.126	5285	1
$\gamma\gamma$	3945	18.5	213	2
$W\gamma$	11375	6.22	1829	1
$b\bar{b}$	4682	35501	0.132	4682
$t\bar{t}$	11149	1682	6.63	222
$\gamma$ -jet	1935	3523	0.549	465

## 6.2 Background measurement from Data

After the selection by the final likelihood at the optimal working points, the  $m_{\gamma\gamma}$  distribution of the background is smooth enough to be easily fit. When the real data will be there, it will be possible to take a  $m_{\gamma\gamma}$  window centred on the  $m_H$  hypothesis, then fit the real data outside this window to estimate the background within the signal window. If the number of events in the sideband is sufficient, this method can be applied and considerably simplify the estimation of the uncertainties on the expected background rate. The MC can be used to optimize the method (size and position of the window, bin width, choice of the fit function...) and to estimate the uncertainty on background: the  $m_{\gamma\gamma}$  distribution is used to generate thousands of signal+background pseudo-experiments. These faked data are fit excluding a mass window around the maximum as shown in Figure 32. The number  $N_{bkg}^{fit}$  of background events in the signal region is given by the integral of the fit function in this mass window. The full statistics MC distribution is fit over the whole mass range. The number  $N_{bkg}^{MC}$  of predicted events in the signal region is the integral of the fit function in the signal mass window. The relative error on the measure is given by the ratio  $N_{bkg}^{fit}/N_{bkg}^{MC}$  and is represented in Figure 33 for 10000 pseudo-experiments for a  $120 \text{ GeV}/c^2$  Higgs boson mass hypothesis and integrated luminosities of  $100 \text{ fb}^{-1}$  and  $300 \text{ fb}^{-1}$ . The mean of the gaussian fit to the  $N_{bkg}^{fit}/N_{bkg}^{MC}$  distribution gives the rescaling factor to apply to background. This factor is related to the width of the signal window. A too narrow window increases this scaling factor, background is surestimated due to the signal events in the tail. A too large window will reduce the precision of the fit. 10000 gedanken experiments have been generated for each  $m_H$  hypothesis at each luminosity point. For all Higgs boson masses, the best results correspond to a symmetric window of  $\pm 8 \text{ GeV}/c^2$ , a bin width of  $4 \text{ GeV}/c^2$  and a second order polynomial

fit function. The relative uncertainty obtained on the background estimation is represented as a function of the luminosity in Figure 34 for a Higgs boson mass of  $120 \text{ GeV}/c^2$ . For a luminosity of  $100 \text{ fb}^{-1}$  and a Higgs boson mass of  $120 \text{ GeV}/c^2$ , the background is measured with a precision of 11%, and with a precision of 6.6% for  $300 \text{ fb}^{-1}$ . The background uncertainty for each  $m_H$  hypothesis can be parametrized by:

$$\frac{\Delta B}{B} = \frac{\alpha(m_H)}{\sqrt{\mathcal{L}}}, \quad \text{with } \mathcal{L} \text{ in } \text{fb}^{-1}$$

The measured  $\alpha(m_H)$  values are given in Table 7.

Table 7: List of the  $\alpha$  parameters used to parametrize the relative uncertainty on the background measured by the sideband fit.

$m_H$	90	100	110	120	130	140	150
$\alpha(m_H)$	0.96	0.96	0.95	1.14	1.13	1.83	1.76

### 6.3 Systematic uncertainties for signal and cross-section measurement

The following sources of error were considered:

- the theoretical cross-section error due to the scale variation: the scales are varied between 0.5 and 2 times the central scales with equal renormalization and factorization scales identified. The central scales for  $V^* \rightarrow VH$  is given by the invariant VH mass. The error is  $\pm 3\%$  for WH and ZH production for all considered Higgs boson masses [12];
- the error on the structure functions of protons: the parton density function of the CTEQ collaboration has been used [27]; The PDF uncertainty for the associated production  $q\bar{q} \rightarrow VH$  at the LHC is almost constant and of the order of 4% over a Higgs boson mass range between 100 and 200  $\text{GeV}/c^2$  [28];
- the error on the measured luminosity is expected to be 3% for luminosity above  $30 \text{ fb}^{-1}$ ;
- the error on the lepton or photon reconstruction and identification has been estimated to 1% for each photon and lepton [29];
- the error on the missing transverse energy: the error amounts to 10% for low  $p_T$  jets and unclustered energy, and to 3% for high  $p_T$  jets. A value of 5% is used and propagated in the final likelihood. This results in a  $-1.08\% +0.49\%$  variation of the final signal rate for  $m_H = 120 \text{ GeV}/c^2$ .

The quadratic sum of all these errors gives a 6% total error on the expected signal rate.

### 6.4 Effect of systematic uncertainties on confidence levels

To propagate the systematic uncertainties on the confidence level, the signal and background expectation values are randomized when computing the probability density functions of the test-statistic as described in [25, 26]. The probability distributions of the systematic uncertainties are assumed to be Gaussian. The systematic uncertainty on the background comes from the sideband fit procedure, described in section 6.2, and is equal to 11 % for a  $120 \text{ GeV}/c^2$  Higgs boson and an integrated luminosity of  $100 \text{ fb}^{-1}$ . The signal systematic uncertainty has both theoretical and instrumental origins, as described in section 6.3, and is equal to 6%. There is no observed effect of the signal systematic uncertainty on the confidence level in the case of signal+background experiments and background-only experiments. Figure 36 shows the statistical significance as a function of the integrated luminosity of the LHC running at high luminosity ( $\mathcal{L} = 10^{34} \text{ cm}^{-2}\text{s}^{-1}$ ). The effect of the systematic uncertainty on the confidence level is represented by the grey band. The loss due to the systematic uncertainty is rather limited: for a  $120 \text{ GeV}/c^2$  Higgs boson, the significance drops from 4.09 to 3.97 for an integrated luminosity of  $100 \text{ fb}^{-1}$ , and from 7.09 to 6.88 for  $300 \text{ fb}^{-1}$ .

## 7 Cross-section measurement

In the case of a Higgs boson discovery, this channel will be used to measure the cross-section times the branching ratio:

$$\sigma_s \times BR = \frac{N_s}{\epsilon_{sel} \mathcal{L}} = \frac{N - N_b^{fit}}{\epsilon_{sel} \mathcal{L}}$$

where  $N_s$  is the number of signal events given by the difference between the total number  $N$  of observed events and the number  $N_b^{fit}$  of background events measured by the sideband fit. The contributions to the total error on the cross-section measurement are the statistical error on the total number of observed events ( $\Delta N = \sqrt{N}$ ), the error on the background estimation with the sideband fit, the error on the measured luminosity and finally the error on the selection efficiency (uncertainty on lepton/photon identification and missing transverse energy, as described in 6.3). The expected precision on the  $\sigma \times BR$  measurement is represented as a function of the integrated luminosity in Figure 35. For a 120 GeV/ $c^2$  Higgs boson, the product of the cross-section and branching ratio will be measured with a precision of 35% after one year of LHC running at high luminosity, and with a precision of 19% after three years of high luminosity running.

## 8 Results for the Standard Model Higgs Boson

Figure 37 represents the statistical significance as a function of  $m_H$  for three luminosity scenario and Figure 38 represents the integrated luminosity required to reach a given statistical significance as a function of  $m_H$ . The bands correspond to the  $1\sigma$  systematic uncertainty. One year of high luminosity running allows an observation at  $3\sigma$  of the SM Higgs boson from the LEP lower limit up to 146 GeV/ $c^2$  and three years of running at high luminosity allows a  $5\sigma$  discovery from the LEP lower limit up to 148 GeV/ $c^2$ .

## 9 MSSM Interpretation

Within the context of the MSSM, the gluon fusion production may be strongly suppressed. The top loop contribution to  $gg \rightarrow h$  may be partially cancelled by the stop loop, when the stop mass is small, *i.e.* for large mixing angle in the stop sector, whereas the partial width  $\Gamma(h \rightarrow \gamma\gamma)$  is dominated by the W boson loop which cannot be cancelled more than 10% by chargino loops for Higgs boson masses greater than 100 GeV/ $c^2$  [3]. For a stop mass of 200 GeV/ $c^2$ , the  $gg \rightarrow \gamma\gamma$  process may be so heavily suppressed that it would be useless for a discovery if  $m_A$  is below 500 GeV/ $c^2$  [30].

The thresholds for 95% CL,  $3\sigma$  and  $5\sigma$  sensitivity for the analysis are shown in Figure 39 as a function of  $m_H$ . The expected  $\sigma \times BR$  for  $WH \rightarrow \nu\gamma\gamma$  as a function of  $m_A$  and  $\tan\beta$  are represented in Figure 40 for no mixing and maximal mixing scenarios. The cross-section sensitivity of the analysis seems to be sufficient to help covering the MSSM parameter space in case of gluophobic scenario, but it has to be confirmed with a detailed study based on a full scan of the MSSM parameter space.

## 10 Conclusion

The possibility to discover a Higgs boson produced in association with a W or Z boson and decaying into two photons has been studied with full simulation and detector response. High luminosity pile-up has been used and both signal and background uncertainties have been included. After three years of LHC running at high luminosity, the SM Higgs boson can be discovered with  $5\sigma$  significance between the 114.4 GeV/ $c^2$  LEP lower limit and 148 GeV/ $c^2$ .

## 11 Acknowledgements

The authors would like to express their thanks to R. Barbier, S. Lowette and S. Nikitenko for their help, advice and constructive remarks.

## References

- [1] M. Pieri *et al.*, “Inclusive search for the Higgs Boson in the  $H \rightarrow \gamma\gamma$  channel”, CMS Note in preparation.
- [2] C. Seez and T.S. Virdee, “Using Tracks to Locate the two Photon Vertex”, **CMS Note 1993/092**;  
C. Seez, “An Algorithm Using Tracks to Locate the two Photon Vertex”, **CMS Note 1993/115**;  
D.J. Graham, “An algorithm using tracks to locate the two photon vertex at high luminosity”, **CMS Note 1995/115**.
- [3] A. Djouadi, “*Squark effects on Higgs boson production and decay at the LHC*”, PM/98-06, [[arXiv:hep-ph/9806315](#)];  
A. Djouadi, *Phys. Lett. B* **435** (1998) 101;  
A. Djouadi *et al.*, “*The coupling of the lightest SUSY Higgs on two photons in the decoupling regime*”, *Eur. Phys. J. C* **1** (1998) 149.
- [4] J.L. Agram *et al.*, “*Associated  $t\bar{t}H$  production with  $H \rightarrow \gamma\gamma$  in CMS*”, CMS Note in preparation.
- [5] M. Dubinin “*Higgs Boson Signal in the reactions  $pp \rightarrow \gamma\gamma + 2$  forward jets*”, **CMS Note 2001/022**;  
M. Dubinin *et al.*, “*The vector boson fusion production with  $H \rightarrow \gamma\gamma$* ”, CMS Note in preparation.
- [6] M. Dubinin *et al.*, “*Light Higgs Boson Signal at LHC in the reaction  $pp \rightarrow \gamma\gamma + \text{jet}$  and  $pp \rightarrow \gamma\gamma + \text{lepton}$* ”, **CMS Note 1997/101**.
- [7] R. Kinnunen and D. Denegri “*Expected SM/SUSY Higgs Observability in CMS*”, **CMS Note 1997/057**.
- [8] Guillaume Eynard, Ph.D. Thesis, “*Etude de la production associée du boson de Higgs  $HW, Ht\bar{t}, HZ \rightarrow \gamma\gamma + e^\pm/\mu^\pm + X$  avec le détecteur ATLAS, auprès du LHC*”, Université Joseph Fourier (1998).
- [9] P-H Beauchemin and G. Azuelos, “*Search for the Standard Model Higgs Boson in the  $\gamma\gamma + E_T^{\text{miss}}$  channel*”, **ATL-PHYS-2004-028**.
- [10] Olivier Ravat, Ph.D. Thesis, “*Etude du Calorimètre électromagnétique de l’expérience CMS et recherche de bosons de Higgs neutres dans le canal de production associée*”, **LYCEN-T2004-29**.
- [11] E. Boos *et al.*, *Nucl. Instr. Meth.* **A534** (2004) 250, [[arXiv:hep-ph/0403113](#)];  
A. Pukhov *et al.*, INP report INP-MSU-98-41-542, [[arXiv:hep-ph/9908288](#)].
- [12] M. Spira, “*QCD Effects in Higgs Physics*”, *Fortsch. Phys.* **46** (1998) 203-284, [[arXiv:hep-ph/9705337](#)];  
T. Han and S. Willenbrock, *Phys. Lett.* **B273** (1991) 167.
- [13] A. Djouadi, J. Kalinowski and M. Spira, “*HDECAY: A program for Higgs Boson Decays in the Standard Model and its Supersymmetric Extension*”, *Comput. Phys. Commun.* **108** (1998) 56, [[arXiv:hep-ph/9704448](#)].
- [14] T. Sjostrand, *Comput. Phys Commun.* **80** (1994) 74;  
S. Mrenna, *Comput. Phys Commun.* **101** (1997) 292;  
T. Sjostrand *et al.*, *Comput. Phys Commun.* **135** (2001) 238, [[arXiv:hep-ph/0010017](#)];  
T. Sjostrand, L. Lonnblat, S. Mrenna and P. Skands, [[arXiv:hep-ph/0308153](#)].
- [15] M. Beneke *et al.*, “*Top quark physics*”, [[arXiv:hep-ph/0003033](#)];  
F. Maltoni, “*Theoretical Issues and Aims at the Tevatron and LHC*”, Hadron Collider Physics Symposium, Les Diablerets, 4-9 July 2005.
- [16] CMSIM, CMS simulation and reconstruction package, <http://cmsdoc.cern.ch/cmsim/cmsim.html>.
- [17] Geant 3, CERN Program Library Long Writeup W5013.
- [18] ORCA, Object Oriented Reconstruction for CMS Analysis, <http://cmsdoc.cern.ch/orca>.
- [19] CMS Collaboration, “*The Tridas Project Design Report, Volume 1: The Trigger Systems*”, **CERN/LHCC 2000/038, CMS TDR 6.1**.
- [20] CMS Collaboration, “*The Tridas Project Design Report, Volume 2: Data acquisition and High-Level Trigger*”, **CERN/LHCC 2002/002, CMS TDR 6.2**.

- [21] E. Meschi *et al.*, "Electron reconstruction in the CMS Electromagnetic Calorimeter", **CMS Note 2001/034**.
- [22] V. Litvin *et al.*, "The rejection of background to the  $H \rightarrow \gamma\gamma$  process using isolation criteria based on information from electromagnetic calorimeter and tracker", **CMS Note 2002/030**.
- [23] M. Pieri *et al.*, "Distinguishing Isolated Photons from Jets", **CMS Note 2006/007**.
- [24] J. D'Hondt *et al.*, "Electron and muon reconstruction in single leptonic  $t\bar{t}$  events", **CMS Note 2006/024**.
- [25] The LEP Higgs Working Group, <http://lephiggs.web.cern.ch/LEPHIGGS/www/Welcome.html>;  
 A.L. Read, "Presentation of search results: the  $CL_s$  technique", *Journal of Physics G: Nucl. Part. Phys.* **28** (2002) 2693;  
 A.L. Read, "Modified Frequentist Analysis of Search Results (The  $CL_s$  Method)", **CERN 2000-005**;  
 T. Junk, "Confidence level computation for combining searches with small statistics", *NIM* **A434** (1999) 435.
- [26] R.D. Cousins and V.L. Highland, "Incorporating systematic uncertainties into an upper limit", *NIM* **A320** (1992) 331.
- [27] The CTEQ collaboration, J. Pumplin *et al.*, "New Generation of Parton Distributions with Uncertainties from Global QCD Analysis", *JHEP* 0207 (2002) 12, [[arXiv:hep-ph/0201195](https://arxiv.org/abs/hep-ph/0201195)].
- [28] A. Djouadi and S. Ferrag, "PDF Uncertainties in Higgs Production at Hadron Colliders", [[arXiv:hep-ph/0310209](https://arxiv.org/abs/hep-ph/0310209)].
- [29] S. Baffioni *et al.*, "Discovery potential for the SM Higgs boson in the  $H \rightarrow ZZ \rightarrow e^+e^-e^+e^-$  decay channel", CMS Note in preparation.
- [30] R. Kinnunen, S. Lehti, A. Nikitenko, S. Rantala, "Effects of large mixing and light stop for  $h \rightarrow \gamma\gamma$  in MSSM", **CMS Note 2000/043**.

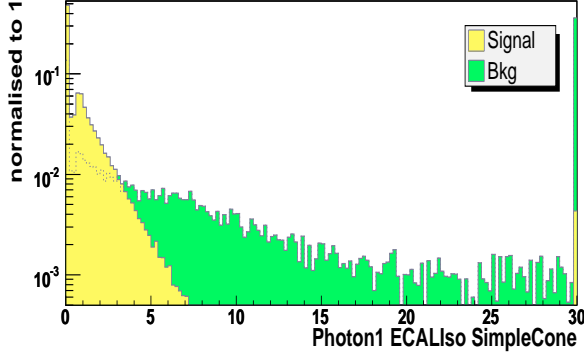


Figure 1: Sum of the transverse energy of island basic clusters with  $\Delta R < 0.3$  from the highest  $E_T$  photon, excluding basic clusters belonging to the photon supercluster at the preselection level.

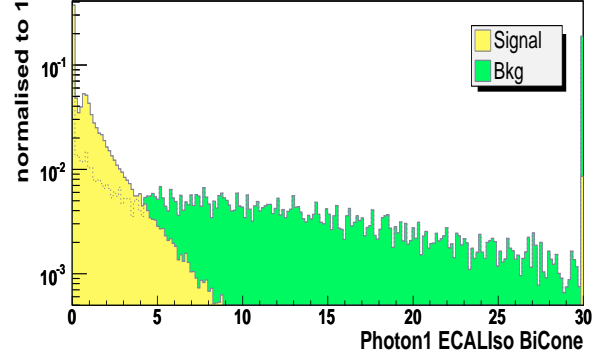


Figure 2: Sum of the transverse energy of island basic clusters with  $0.08 < \Delta R < 0.3$  from the highest  $E_T$  photon at the preselection level.

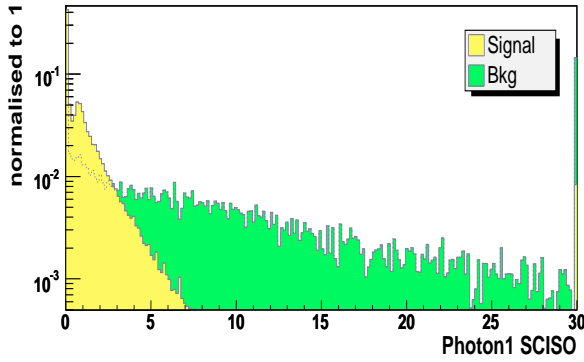


Figure 3: Sum of the transverse energy of island basic clusters with  $0.08 < \Delta R < 0.35$  from the highest  $E_T$  photon, excluding basic clusters in a  $|\Delta\eta| < 0.03$  ring at the preselection level.

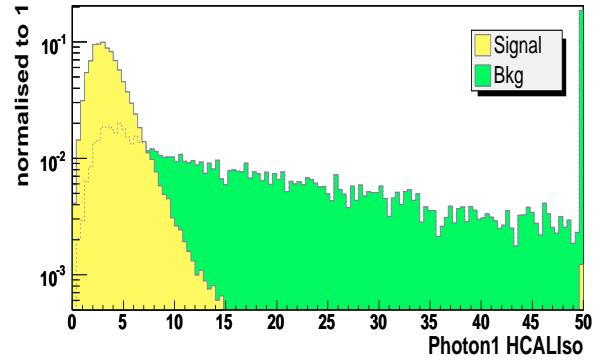


Figure 4: Sum of the transverse energy of the HCAL towers with  $\Delta R < 0.3$  from the highest  $E_T$  photon at the preselection level.

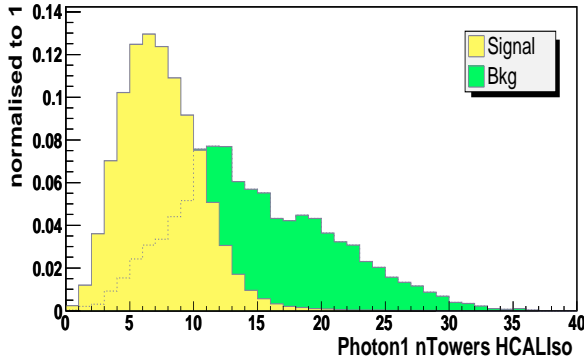


Figure 5: Number of HCAL towers hit within a cone  $\Delta R < 0.3$  around the highest  $E_T$  photon at the preselection level.

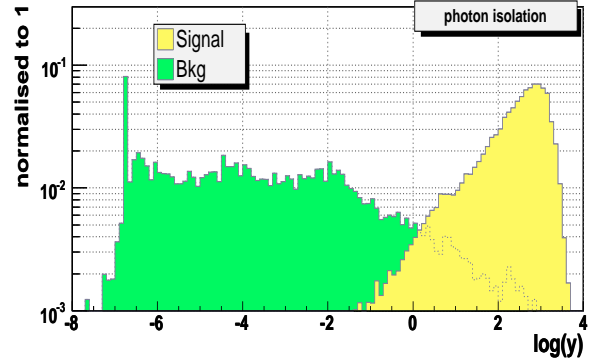


Figure 6: Combined likelihood variable used in photon isolation. The cut  $\log(y_1) > -0.4$  is applied in the analysis.

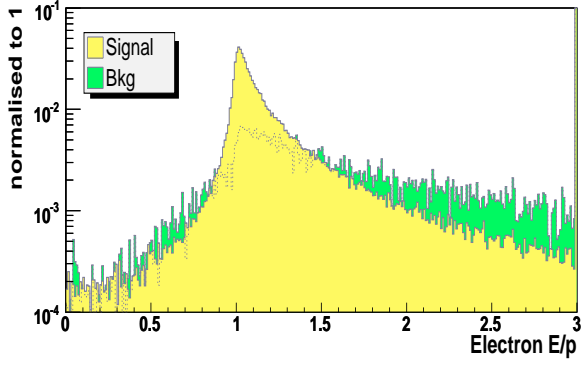


Figure 7: Ratio of the electron calorimeter energy over its tracker momentum at the preselection level.

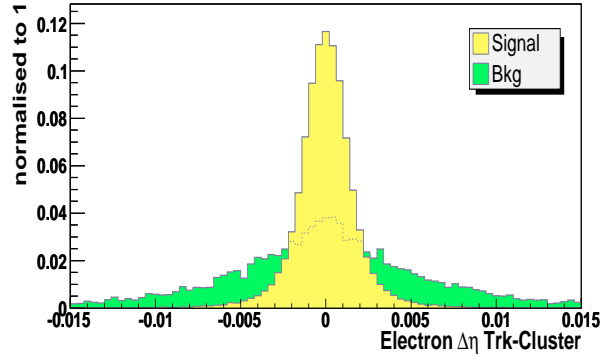


Figure 8:  $\Delta\eta$  between the electron track and its matching supercluster at the preselection level.

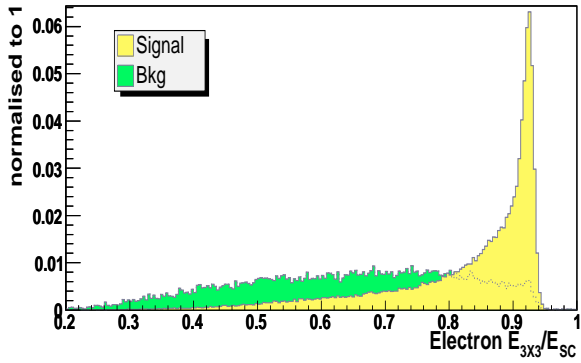


Figure 9: Ratio of the energy sum of  $3 \times 3$  crystals over supercluster energy at the preselection level.

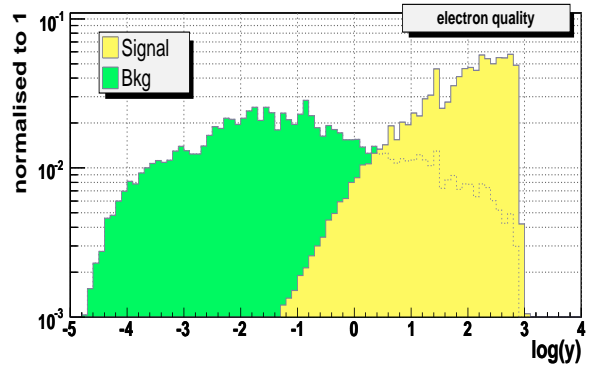


Figure 10: Distribution of the combined likelihood variable reflecting the quality of the electron reconstruction. The cut  $\log(y_2) > -0.6$  is applied in the analysis.

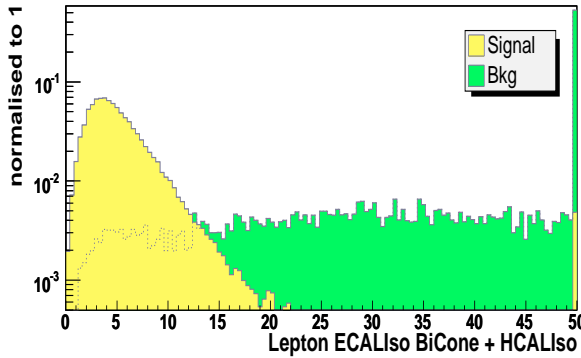


Figure 11: Sum of the transverse energy of island basic clusters in a cone  $0.08 < \Delta R < 0.3$  around the lepton is added to the sum of the transverse energy of the HCAL towers in a cone  $\Delta R < 0.3$  around the lepton. The distributions are shown at the preselection level.

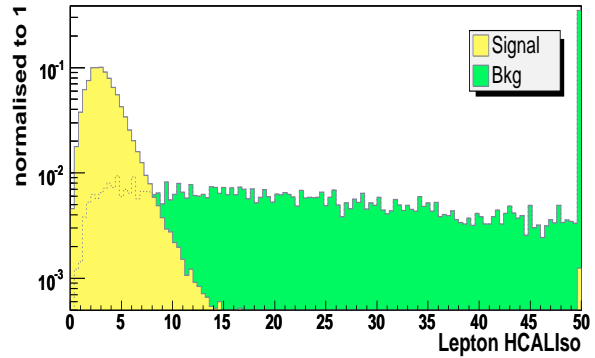


Figure 12: Sum of the transverse energy of the HCAL towers in a cone  $\Delta R < 0.3$  around the lepton at the preselection level.

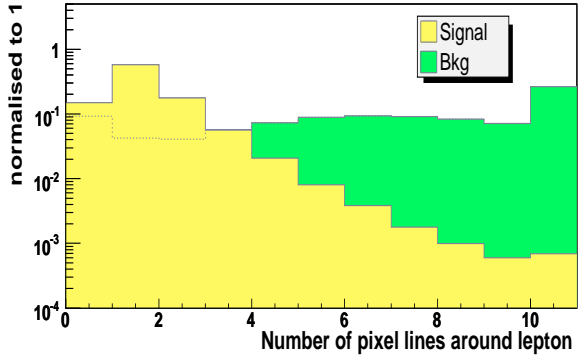


Figure 13: Number of pixel lines in a cone  $\Delta R < 0.3$  around the lepton at the preselection level.

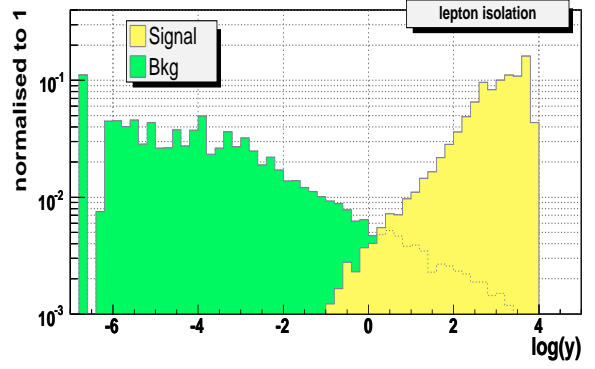


Figure 14: Distribution of the combined variable used for lepton isolation. The cut  $\log(y_3) > -0.3$  is applied in the analysis. The discontinuities observed on the distributions are due to the use of a discrete variable (the number of pixel lines around lepton) in the likelihood.

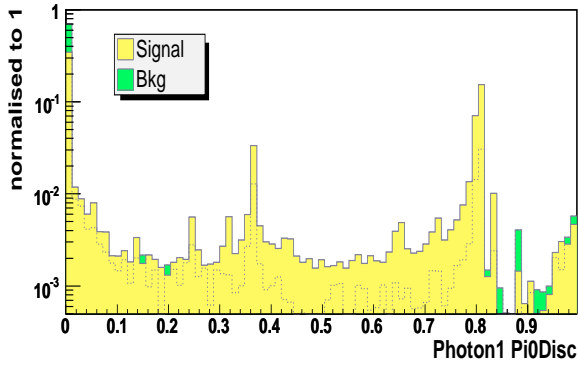


Figure 15: Output of the standard ORCA  $\pi^0$  discriminator applied to the first photon at the preselection level.

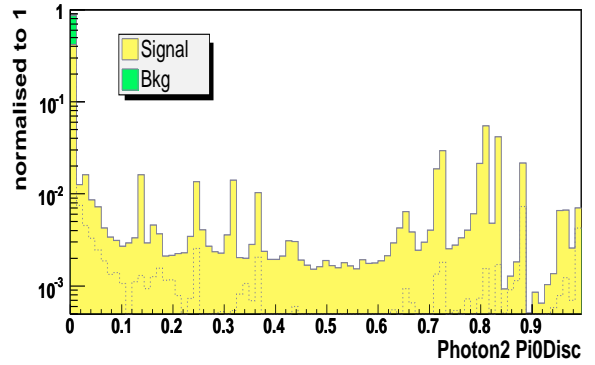


Figure 16: Output of the standard ORCA  $\pi^0$  discriminator applied to the second photon at the preselection level.

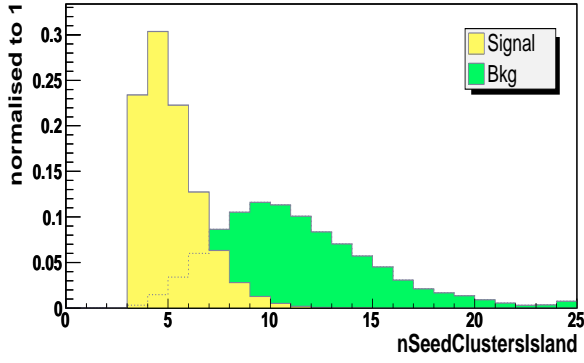


Figure 17: Number of seed clusters reconstructed with the Island algorithm at the preselection level.

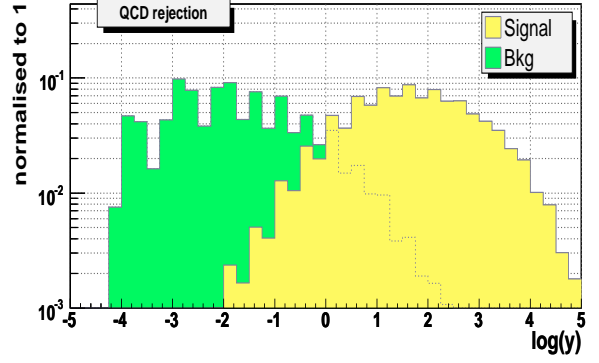


Figure 18: Distribution of the combined variable used to reject multijet events. The discontinuities observed on the distributions are due to the use of discrete variables in the likelihood. The cut  $\log(y_4) > -0.8$  is applied in the analysis.

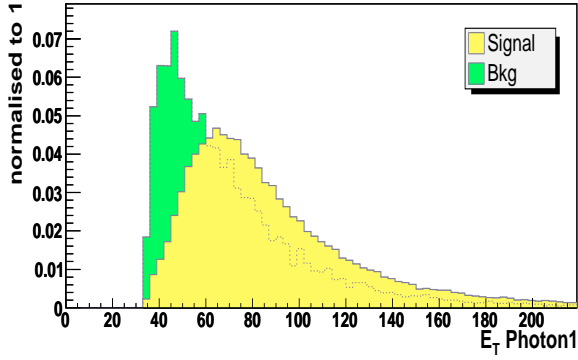


Figure 19: Transverse energy of the highest  $E_T$  photon before the final likelihood selection.

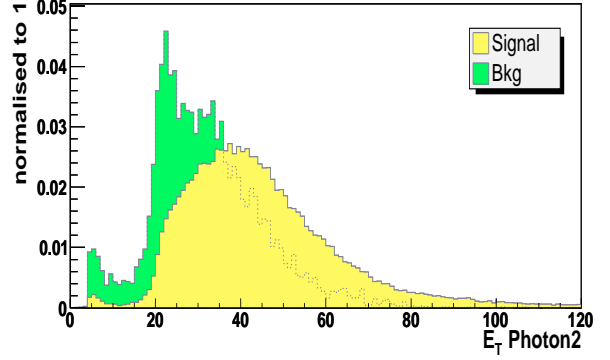


Figure 20: Transverse energy of the second highest  $E_T$  photon before the final likelihood selection.

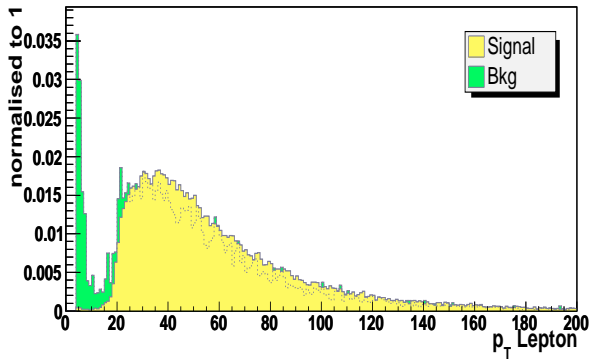


Figure 21: Transverse energy of the selected lepton before the final likelihood selection.

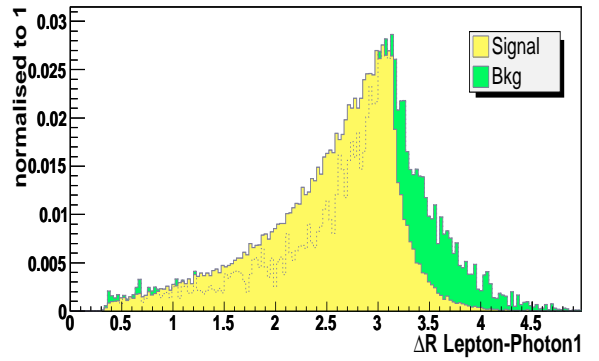


Figure 22:  $\Delta R$  distance between the lepton and the highest  $E_T$  photon before the final likelihood selection.

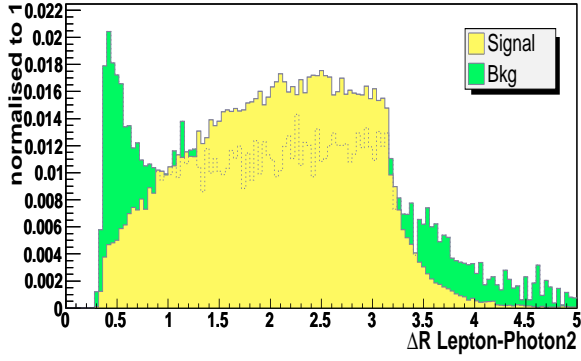


Figure 23:  $\Delta R$  distance between the lepton and the second highest  $E_T$  photon before the final likelihood selection.

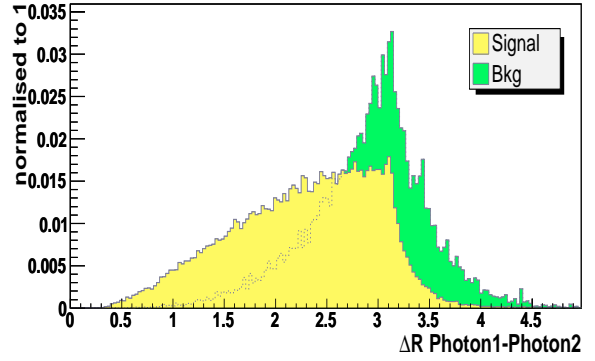


Figure 24:  $\Delta R$  distance between the two photons before the final likelihood selection.

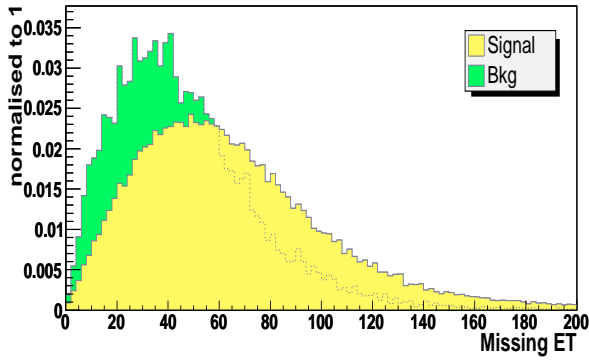


Figure 25: Missing transverse energy before the final likelihood selection.

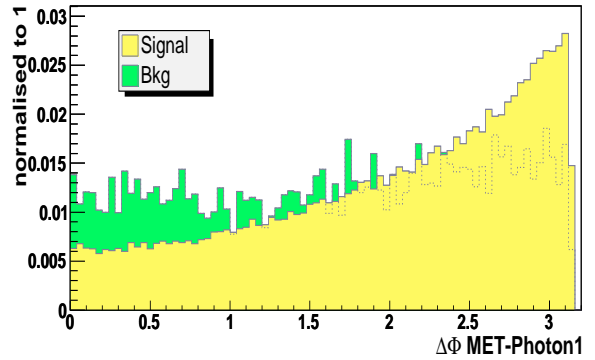


Figure 26:  $\Delta\Phi$  between missing energy direction and highest  $E_T$  photon before the final likelihood selection.

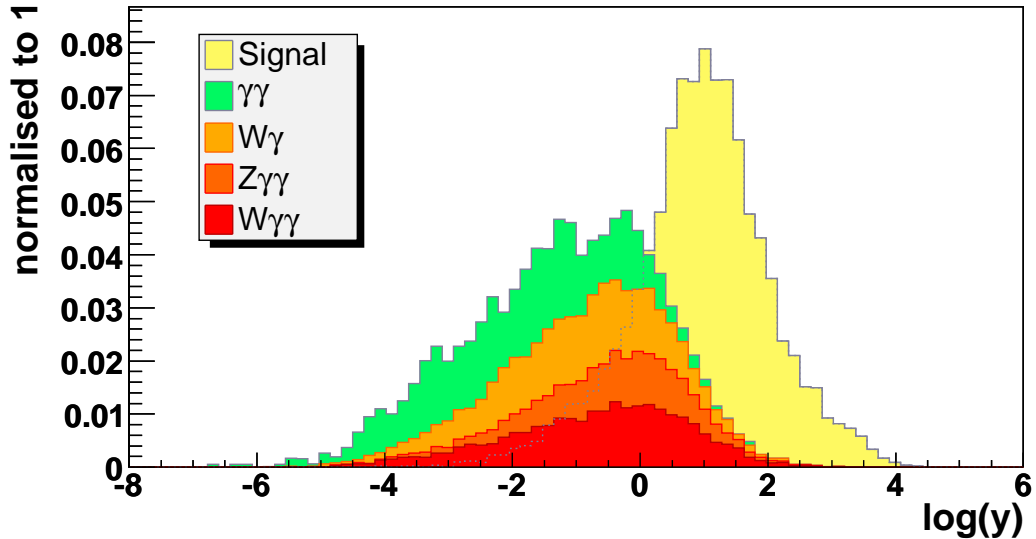


Figure 27: Distribution of the kinematical combined variable  $y_5$  for the signal ( $m_H = 120 \text{ GeV}/c^2$ ) and for the background. The optimal working point is obtained with a cut  $\log(y_5) > 0.35$ .

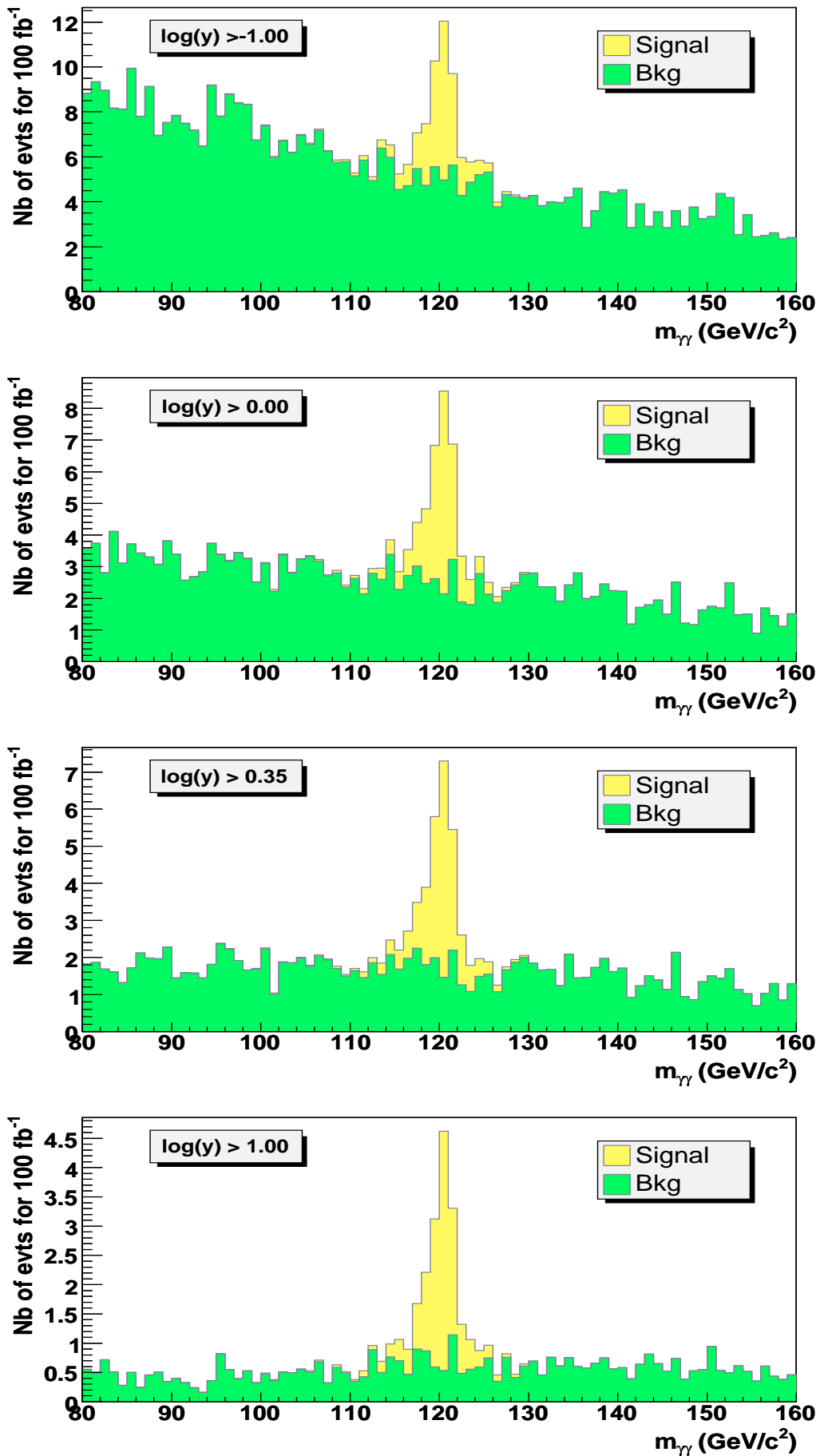


Figure 28: Reconstructed  $\gamma\gamma$  mass for a  $120 \text{ GeV}/c^2$  Higgs boson signal (light grey) and for background (dark grey) after different cuts on the final likelihood output variable  $y_5$ .

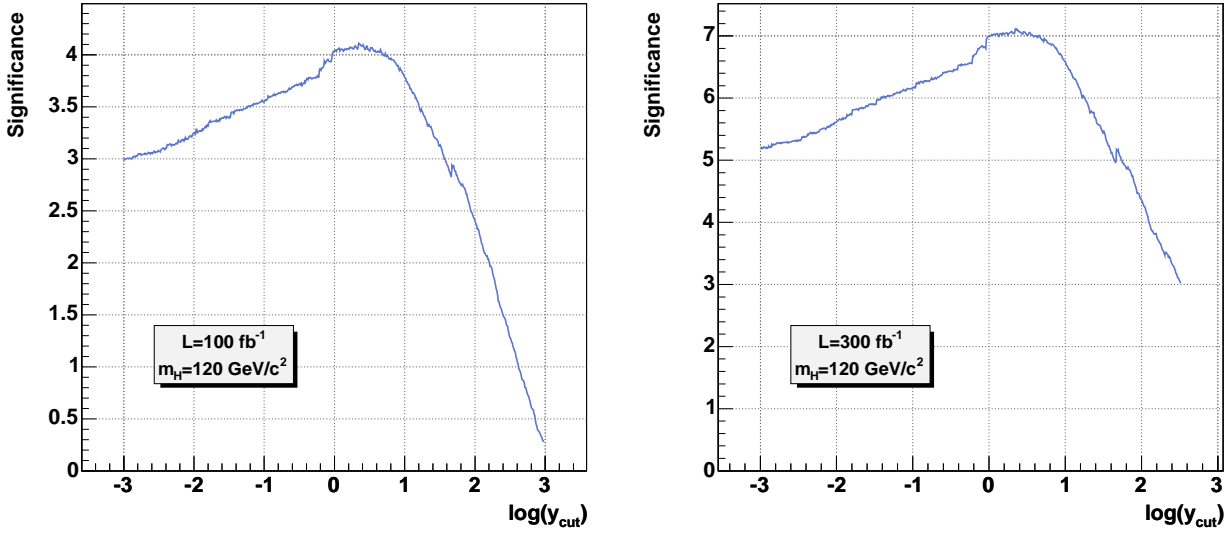


Figure 29: Statistical significance as a function of the cut on the final combined variable  $\log(y_5)$ , for  $m_H = 120 \text{ GeV}/c^2$  and for integrated luminosities of  $100 \text{ fb}^{-1}$  (left) and  $300 \text{ fb}^{-1}$  (right).

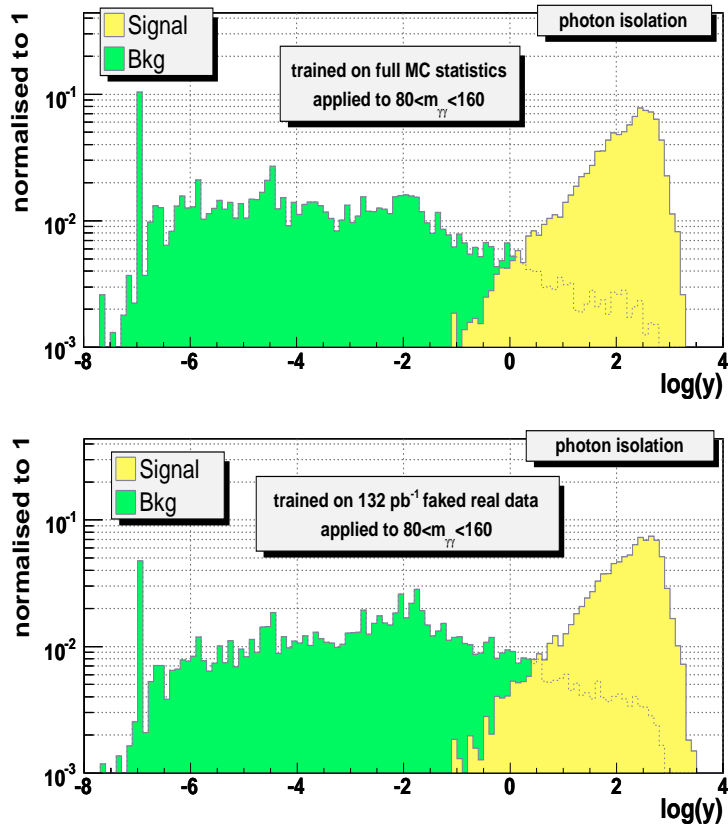


Figure 30: Distribution of the photon isolation combined variable  $y_1$  obtained by the standard analysis using the full MC statistics (top) and obtained by optimizing the likelihood with a sample of  $132 \text{ fb}^{-1}$  of “fake real data” taken in the  $20 < m_{\gamma\gamma} < 80 \text{ GeV}/c^2$  sideband (bottom). In this last case, the increase of the background tail in signal region is mainly due to  $\gamma$ -jet and  $t\bar{t}$  events.

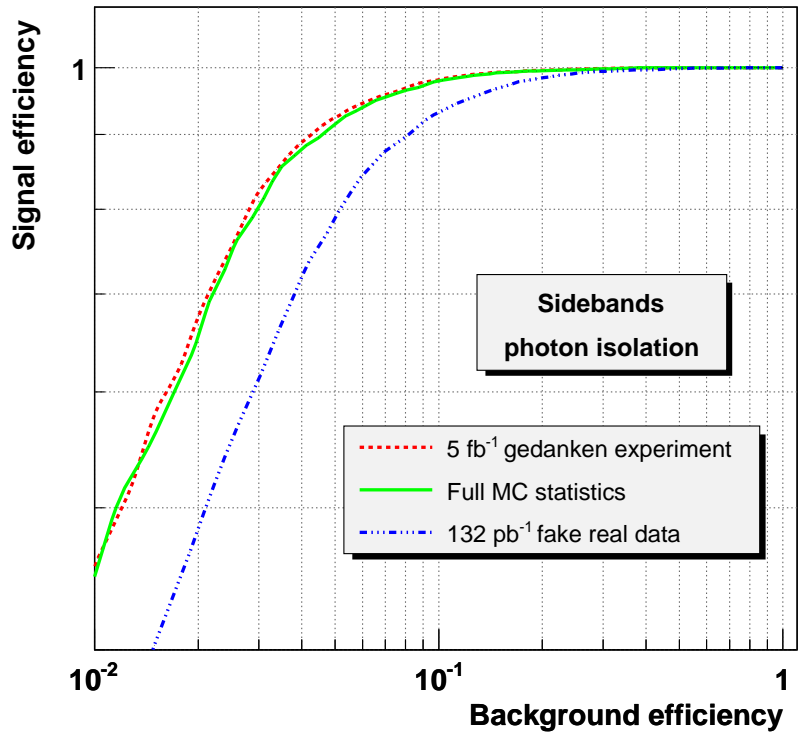


Figure 31: Comparison of the performance obtained when optimizing the photon isolation likelihood with a sample of  $132 \text{ fb}^{-1}$  of “fake real data” taken in the  $20 < m_{\gamma\gamma} < 80 \text{ GeV}/c^2$  sideband (dash-dotted line) with the performance obtained by the standard analysis using the full MC statistics (solid line). To increase the available statistics in the sideband, gedanken experiments were generated for an equivalent luminosity of  $5 \text{ fb}^{-1}$ . The results of the optimization on these sideband events is represented by the dotted line.

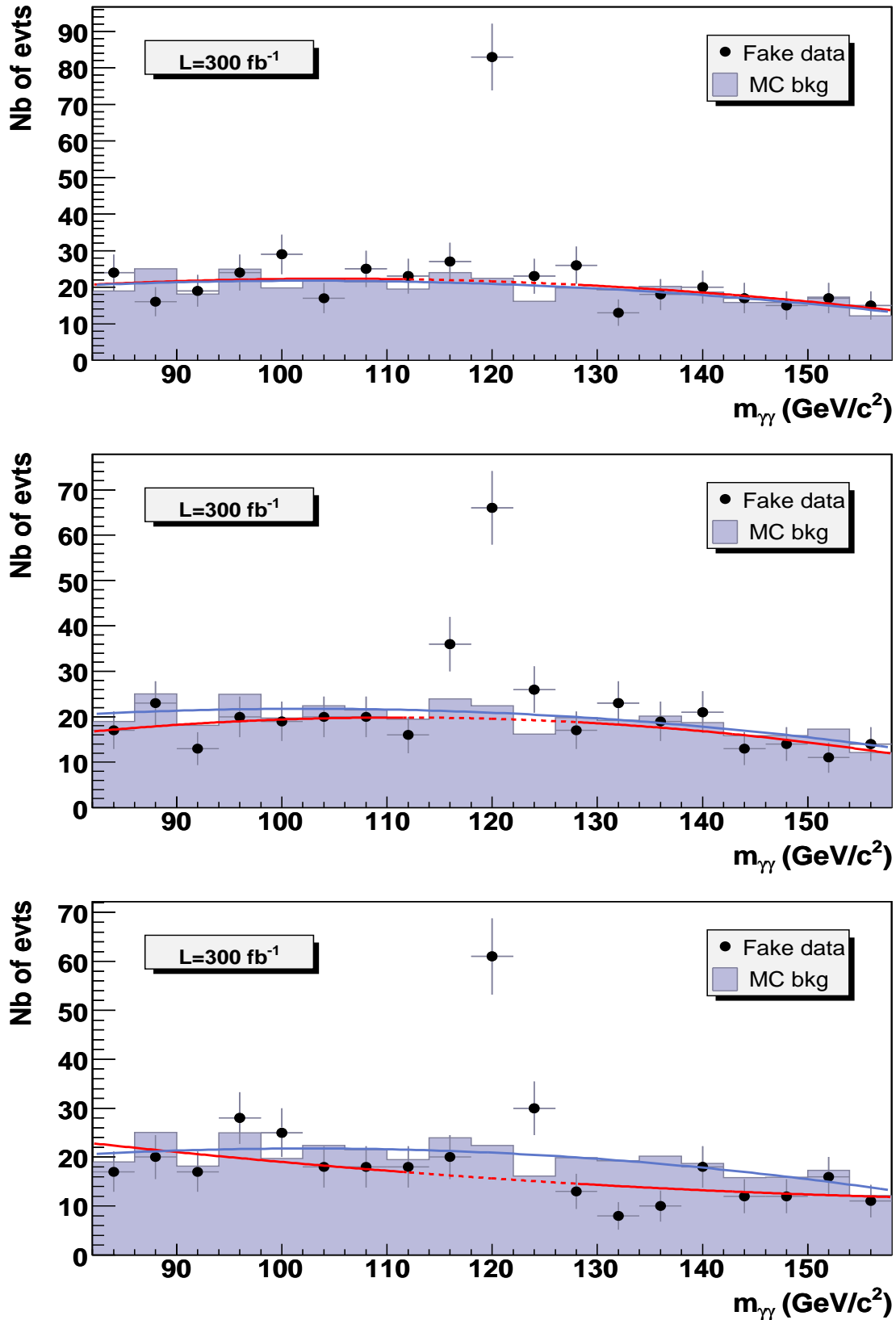


Figure 32: Background measurement in the signal region with a fit on the  $m_{\gamma\gamma}$  sideband. The fit of the full MC statistics over the whole mass range is represented by the solid light gray line. The fit of the fake data (dark grey) is performed on the sidebands, *i.e.* after the exclusion of the signal window represented by the dotted line. The number of background events in the signal region is given by the integral of the fit function in this window. Three gedanken experiments are represented for an integrated luminosity of  $300 \text{ fb}^{-1}$  and a  $120 \text{ GeV}/c^2$  Higgs boson mass hypothesis, one gives a good accuracy of the background estimation (2.9%, top plot), one a typical precision (6.9%, middle plot) and the last a poor estimation (17.1%, bottom plot).

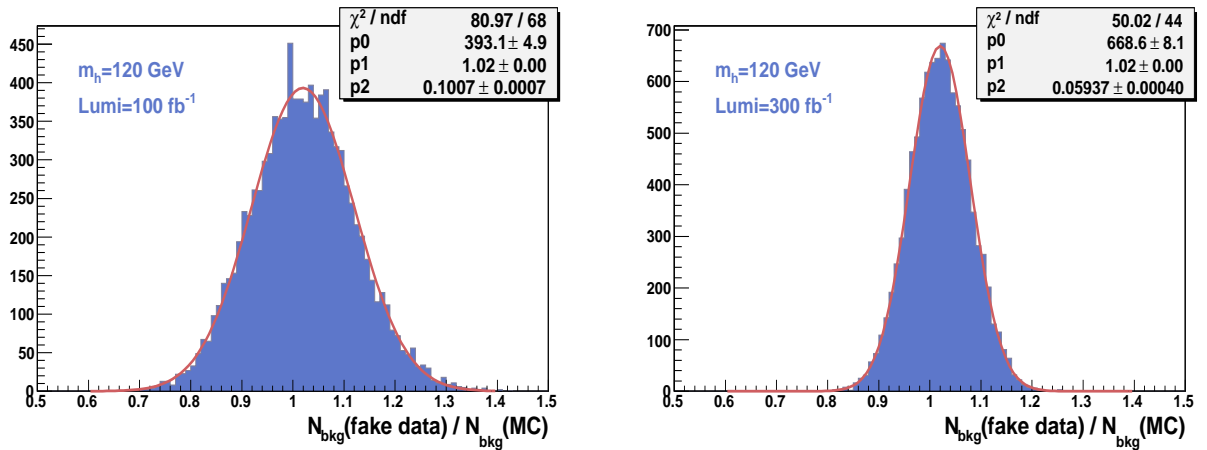


Figure 33: Ratio between the number of background events in the signal region estimated by the fit of real data in sideband and the number of expected background events given by the full statistics MC for  $m_H = 120 \text{ GeV}/c^2$  and integrated luminosities of  $100 \text{ fb}^{-1}$  (left) and  $300 \text{ fb}^{-1}$  (right).

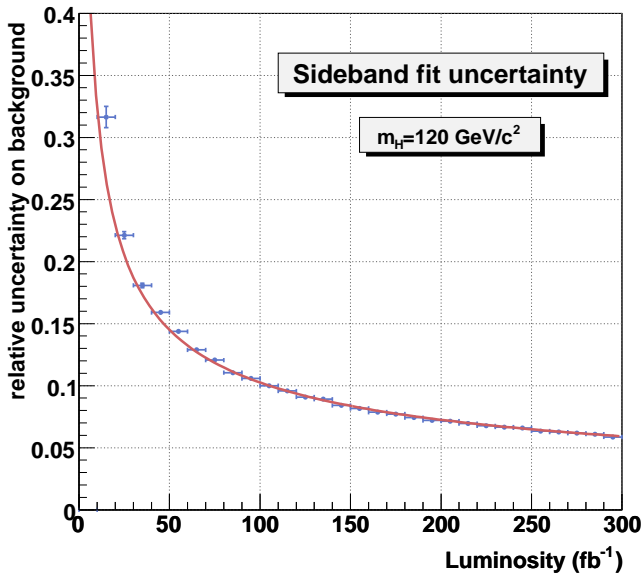


Figure 34: Relative uncertainty on the background estimation by the sideband fit method as a function of the integrated luminosity with LHC running at high luminosity for a Higgs boson mass of  $120 \text{ GeV}/c^2$ .

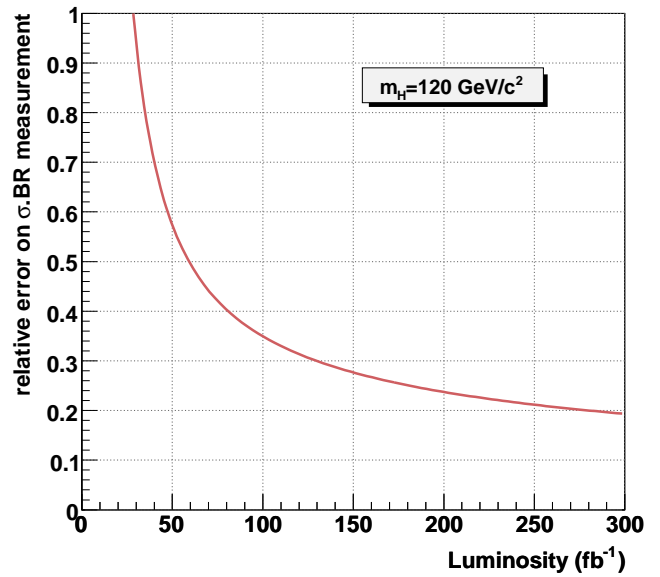


Figure 35: Precision on the measurement of the product of cross-section and branching ratio as a function of the integrated luminosity with LHC running at high luminosity for a  $120 \text{ GeV}/c^2$  Higgs boson.

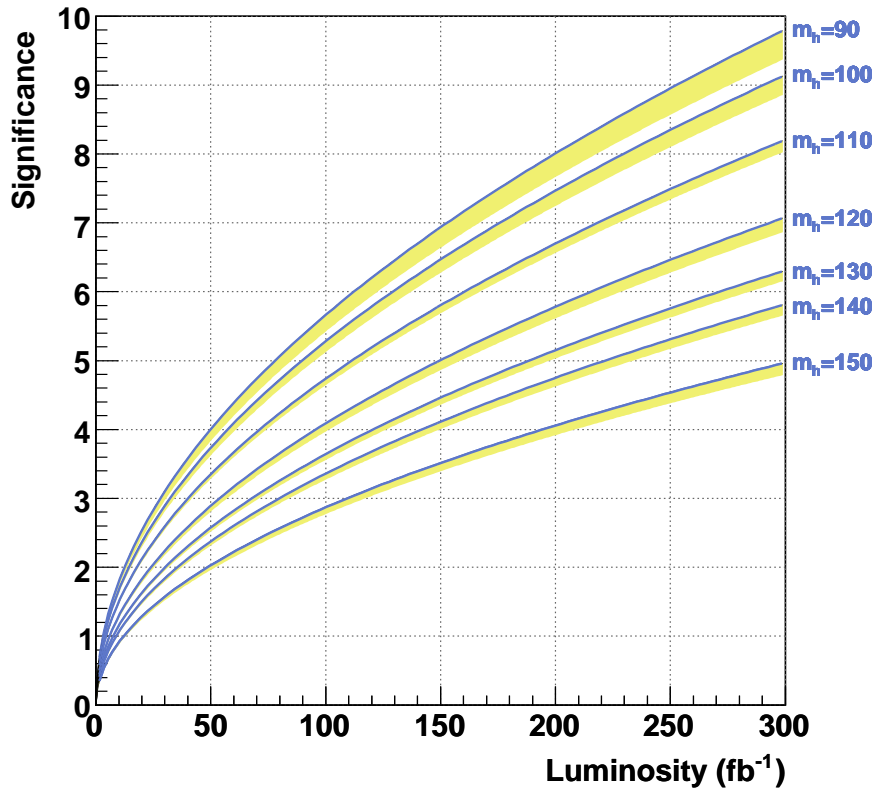


Figure 36: Statistical significance for different Higgs boson mass hypotheses as a function of the integrated luminosity with LHC running at high luminosity. The  $1\sigma$  systematic uncertainty is represented by the grey band.

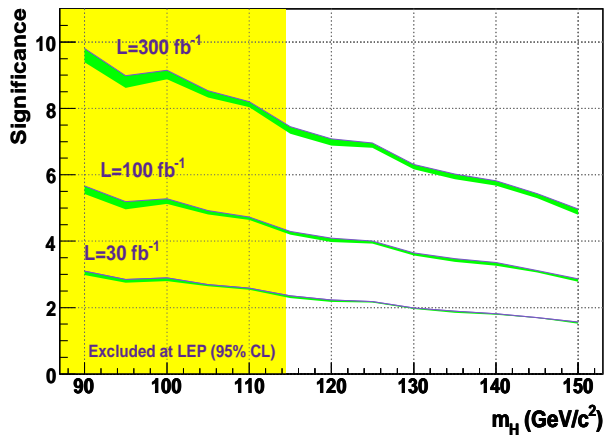


Figure 37: Statistical significance as a function of  $m_H$  after  $30\text{ fb}^{-1}$ , 1 year and 3 year of high luminosity running. The  $1\sigma$  systematic uncertainty is represented by the grey band.

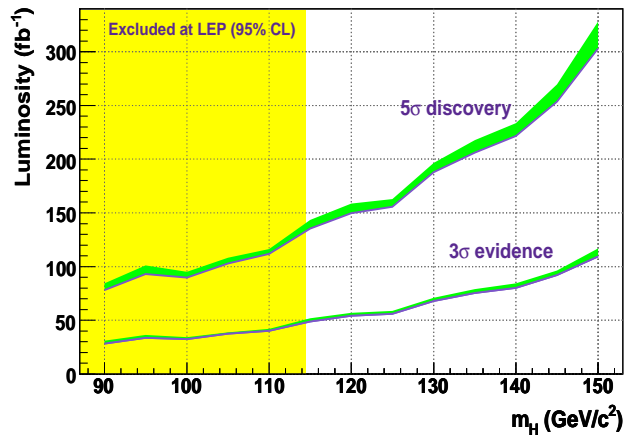


Figure 38: Integrated luminosity needed for a  $5\sigma$  discovery, and for a  $3\sigma$  observation as a function of  $m_H$ . The  $1\sigma$  systematic uncertainty is represented by the grey band.

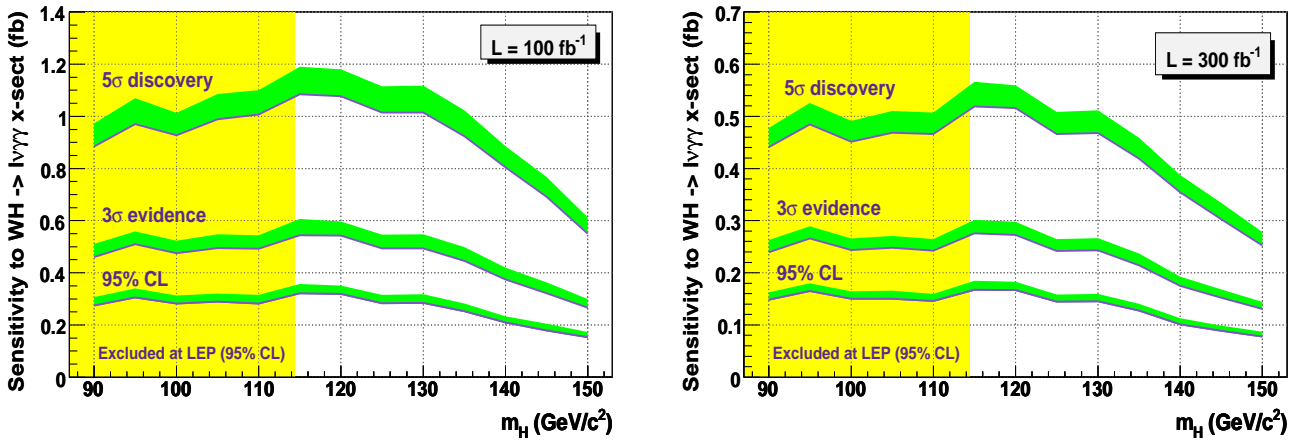


Figure 39: Analysis sensitivity to the  $WH \rightarrow l\nu\gamma\gamma$  cross-section as a function of  $m_H$  after one year (left) and three years (right) of high luminosity running. The  $1\sigma$  systematic uncertainty is represented by the grey band.

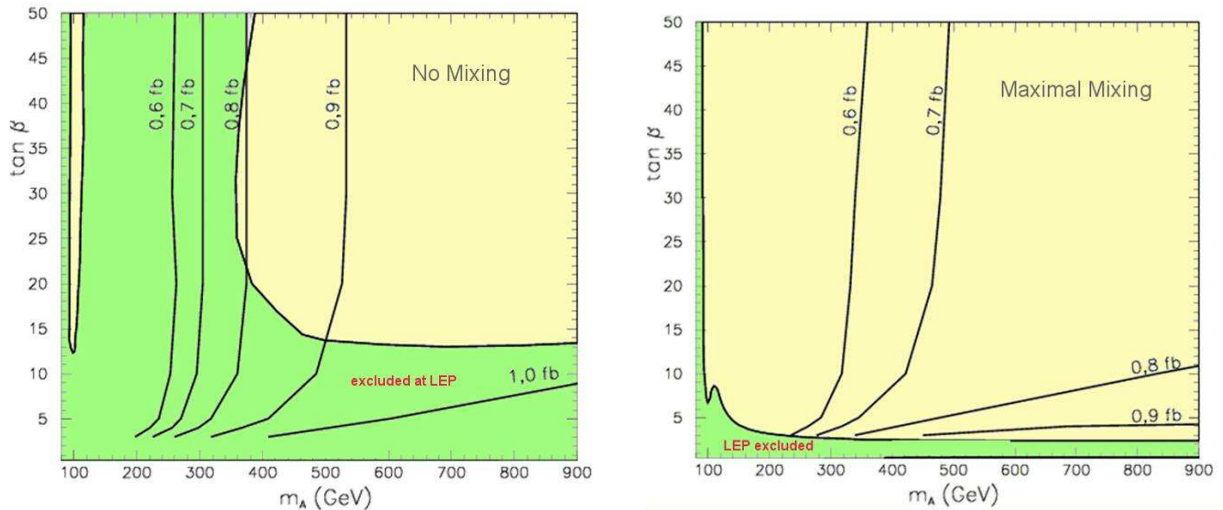


Figure 40: Expected cross-sections for  $WH \rightarrow l\nu\gamma\gamma$  as a function of  $m_A$  and  $\tan \beta$  in the no mixing scenario (left) and in the maximal mixing scenario (right) of the MSSM.